Radiative intersubband polaritons and reflection-absorption spectra of asymmetric microcavities with embedded multiple quantum wells

M. Załużny and W. Zietkowski
Institute of Physics and Nanotechnology Center, Maria Curie-Skłodowska University, Pl. M. Curie-Skłodowskiej 1, 20-031 Lublin, Poland
(Received 11 January 2008; revised manuscript received 20 May 2008; published 21 July 2008)

The usefulness of the concept of constant angle radiative intersubband polaritons in the description of the behavior of reflection-absorption spectra of bulk asymmetric microcavities with embedded multiple quantum wells is demonstrated. It is shown that a recently observed complex of the triple peaked absorption spectra of the above mentioned structures can be well reproduced employing expressions for the contribution of a single polariton mode to the microcavity absorption. The physical origin of the polariton modes responsible for the different peaks is also discussed.

DOI: 10.1103/PhysRevB.78.033305 PACS number(s): 78.67.De, 71.36.+c

In the past two decades, remarkable progress has been made in the understanding of the coupling of infrared radiation to intersubband transitions in single n-doped quantum wells (QWs).[1] However, the physics associated with the intersubband optical response of multiple quantum well (MQW) structures embedded into multilayered systems is still far from complete understanding. The problem seems to be particularly interesting in the case of bulk asymmetric microcavities (BAMCs) where the active material, i.e., MQW, extends over the whole length between mirrors. In such a type of cavities the complex of the triple peaked absorption spectra was recently observed by Dupont *et al.*[2,3] The authors successfully reproduced the angle-resolved reflection-absorption (ARRA) spectra employing the transfer-matrix formalism and the effective-medium approximation.[4] Unfortunately, such an approach does not allow for detailed clarifications of what kind of quasinormal modes (QNMs) of the sample are responsible for the above mentioned multiple peak features.[5–7] In this Brief Report we present a semiclassical analysis showing that multiple peak features appearing in the ARRA spectra of the BAMCs can be described in terms of constant angle intersubband cavity polaritons. The nature of the polariton modes responsible for the different peaks is also discussed.

Let us assume that a layered structure, with embedded MQW, is sandwiched between a semi-infinite substrate (ε_s) and cladding (ε_c) media. The monochromatic light (with the $e^{-i\omega t}$ time dependence and the polarization in the x-z plane) incidents from the nonabsorbing substrate medium at the angle φ with respect to the optic axis z oriented parallel to the growth direction. In this configuration there is only a single component of the magnetic field. The general expression for the 2×2 transfer matrix ($\mathbf{T}$) connecting the magnetic-field amplitudes in cladding and substrate media can be calculated by modeling the MQW by an effective uniform uniaxial medium with the diagonal dielectric tensor $\varepsilon_{ij}=\delta_{ij}\varepsilon_{ii}$.[4] Once the $\mathbf{T}$ matrix is known the overall reflection coefficient of the structure (r) is calculated as $r=T_{21}/T_{11}$.

The dispersion relations for the QNMs supported by the whole structure can be derived from the requirement $T_{11}=0$ equivalent to the so-called outgoing boundary conditions.[7] The above equation can be numerically solved, e.g., with a Muller algorithm. We will focus on solutions corresponding to a typical total internal reflection geometry, i.e., we assume that QNMs radiate energy into the substrate (only) at a fixed angle φ. It is well known that the eigenfrequency of the (nonstationary) QNM is a complex quantity. However, when the in-plane wave vector of the mode is taken real, the uncertainty in the mode frequency leads to an angular spread in the radiating fields. In order to overcome this problem we assume, solving the dispersion equation, that the mode frequency ($\tilde{\omega}_\nu$) and its wave vector ($\tilde{k}_x$) are complex quantities with the same phase in the complex plane, i.e., $\tilde{k}_x/\tilde{\omega}_\nu=|\tilde{k}_x/\tilde{\omega}_\nu|$.[5] Such a type of constant angle virtual modes can be directly connected with the features in the ARRA spectra.

The case when the νth QNM mode is spectrally separated from the rest of the modes is especially interesting. Then, for ω close to Re $\tilde{\omega}_\nu$ the absorptance $A=1-|r|^2$ of the structure is determined mainly by the resonant contribution from the above mentioned mode. One can show (details will be published) that this contribution takes the following Lorentzian form:

$$A_\nu=\mathcal{A}_\nu\frac{1}{[(\omega-\omega'_\nu)/\omega''_\nu]^2+1}, \tag{1}$$

where $\mathcal{A}_\nu=4(\mathcal{R}_\nu-\mathcal{R}_\nu^2)$ and $\mathcal{R}_\nu=\omega''_\nu/\omega''_\nu$. $\tilde{\omega}_\nu=\omega'_\nu+i\omega''_\nu$ ($\tilde{\omega}_\nu=\omega'_\nu+i\omega''_\nu$) denotes the mode frequency obtained including (neglecting) dissipation in all constituent materials. Two particular examples of the multiple absorption peaks in the ARRA spectra of the BAMCs and their interpretation through Eq. (1) are presented below.

At first we discuss the BAMC (with metallic cladding) similar to the one studied recently by Dupont *et al.*[2] The sample is grown on a GaAs semi-insulating substrate ($\varepsilon_s=\varepsilon_{\mathrm{GaAs}}$) and consists of a 140-repeat ($N_{\mathrm{QW}}=140$) MQW embedded between a 0.4-μm-thick n^+ GaAs top layer and 0.8-μm-thick n^+ GaAs bottom layer with the doping concentration $N_D=2\times 10^{18}$ cm^{-3}. The cladding medium is Au. The period of the MQW consists of a 60-Å GaAs QW and a 290-Å $Al_{0.21}Ga_{0.79}As$ barrier. The QW is treated as a two subband system with the intersubband plasmon energy $E_{\mathrm{IT}}=\hbar\omega_{\mathrm{IT}}=114$ meV, and the homogeneous linewidth $2\hbar\gamma_{\mathrm{IT}}=2.2$ meV. The product of the intersubband oscillator

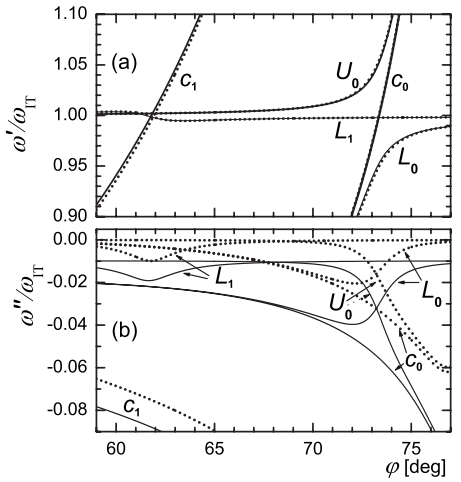

FIG. 1. (a) The real and (b) imaginary part of the frequencies of the modes c_0, c_1, U_0, L_0, and L_1 supported by the metal clad microcavity described in the text as a function of φ. The solid (dotted) curves are obtained including (neglecting) the dissipation in constituent materials.

strength $f_{\rm osc}$ and the surface electron density N_s is taken to be $\mathcal{N}_s=N_s f_{\rm osc}=2\times10^{10}$ cm^{-2}. (For simplicity we neglect the intrasubband transitions since they have a negligible influence on the reflection spectra of the structures considered in this Brief Report.) The numerical values of the material parameters are taken the same as in Ref. 2. The angular dependences of the two lowest photonic modes (c_0 and c_1) supported by the passive cavity ($N_s=0$) are presented in Fig. 1. We find that the resonance condition $\omega'_{c_0}=\omega_{\rm IT}$ ($\omega'_{c_1}=\omega_{\rm IT}$) is achieved at $\varphi=\varphi^{(0)}_{\rm res}\cong73.35°$ [$\varphi=\varphi^{(1)}_{\rm res}\cong61.8°$]. The quality factor $Q^{(i)}(\equiv\omega'_{c_i}/2|\omega''_{c_i}|)$ is then rather small $Q^{(1)}_{\rm res}\cong10$ [$Q^{(2)}_{\rm res}\cong6$]. The coupling between the intersubband electronic modes and photonic modes leads to the formation of the cavity polaritons. Figure 1 displays the behavior of three polariton modes (denoted by U_0, L_0, and L_1), which can be associated with the features in the ARRA spectra observed at $\varphi\approx\varphi^{(0)}_{\rm res}$. For the sake of clarity nearly dispersionless modes located slightly below $\omega_{\rm IT}$ and denoted by $L_{i>1}$ are not presented in the above figure.

Figure 2 illustrates the fact that all three absorption peaks predicted by the transfer-matrix method are well reproduced by Eq. (1). We assign two large peaks to the U_0 and L_0

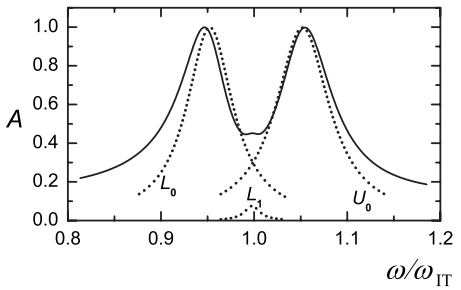

FIG. 2. The spectral dependence of the absorptance of the BAMC discussed in Fig. 1 at $\varphi=\varphi^{(0)}_{\rm res}=73.35°$. The solid (dotted) curves are obtained employing the transfer-matrix approach [Eq. (1)].

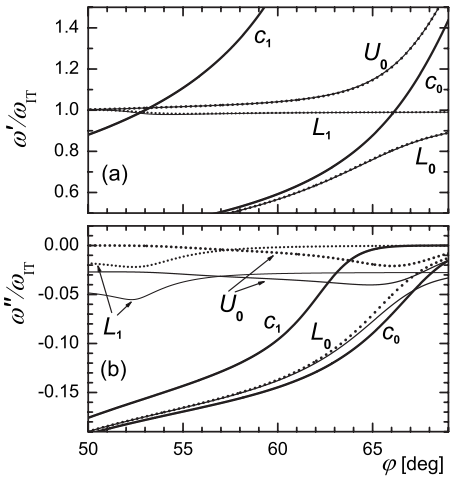

FIG. 3. (a) The real and (b) imaginary part of the frequencies of the modes c_0, c_1, U_0, L_0, and L_1 supported by the dielectric microcavity described in the text as a function of φ. The solid (dotted) curves are obtained including (neglecting) the dissipation in constituent materials.

modes. The small central peak is mainly due to the L_1 mode.

Below we discuss the microcavity (with purely dielectric mirrors), which is similar to the one studied recently by Plumridge *et al.*[8] It is grown on a GaAs substrate ($\varepsilon_s=\varepsilon_{\rm GaAs}$) and consists of a MQW (with $N_{\rm QW}=50$) embedded between $Al_{0.1}Ga_{0.9}As$ top and bottom layers with thicknesses $d_t=2.6$ μm and $d_b=2.2$ μm, respectively. The cladding medium is air ($\varepsilon_c=1$). The period of the MQW consists of a 60-Å GaAs QW and a 300-Å $Al_{0.35}Ga_{0.65}As$ barrier. The QW is treated as a two subband system with $E_{\rm IT}=136$ meV, $2\hbar\gamma_{\rm IT}=7.6$ meV, and $\mathcal{N}_s=6.5\times10^{11}$ cm^{-2}. (The material parameters are taken the same as in Ref. 8.) Figure 3 presents the angular dependence of the QNMs supported by the passive and active microcavity. (The mode notation is the same as in Fig. 1.) We find that the resonance condition $\omega'_{c_0}=\omega_{\rm IT}$ ($\omega'_{c_1}=\omega_{\rm IT}$) is now achieved at $\varphi=\varphi^{(0)}_{\rm res}\cong66.2°$ [$\varphi=\varphi^{(1)}_{\rm res}\cong53°$]. The quality factor is about two times smaller than in the previous system.

The behavior of the polariton modes in both of the considered systems is qualitatively similar. Nevertheless, some differences are easily observable. For example in Fig. 3, the anticrossing of the curves ω'_{L_0} and ω'_{U_0} is not accompanied by the crossing [at $\varphi=\varphi^{(0)}_{\rm res}$] of the curves ω''_{L_0} and ω''_{U_0}. Moreover, the cavity mode broadening $\gamma_i=|\omega''_{c_i}|$ does not increase (such as in Fig. 1) but decreases with increasing φ. It seems that the above mentioned differences can be partially associated with the fact that the reflectivity of the cavity mirrors and penetration of the cavity modes inside them depend strongly on φ and ω. As one can expect, the features in ARRA spectra obtained employing the transfer-matrix method (see Fig. 4) are well reproduced by Eq. (1).

To get useful analytical results, allowing for a simple and intuitive physical interpretation of the behavior the intersubband polariton modes supported by bulk microcavities, we now discuss the simplest possible model—a $\lambda/2$ cavity. It is composed of the MQW, with thickness $d_{\rm MQW}$ and $N_{\rm QW}\gg1$, bounded by metallic mirrors located at $z=\pm L_{\rm cav}/2$.[9,10] (The

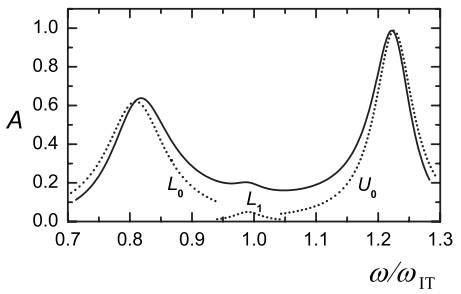

FIG. 4. The spectral dependence of the absorptance of the BAMC discussed in Fig. 3 at $\varphi=\varphi_{\rm res}^{(0)}=66.2°$. The solid (dotted) curves are obtained employing the transfer-matrix approach [Eq. (1)].

main conclusions will be valid also in the case of dielectric mirrors.) In the limit of perfect metallic mirrors ($\gamma_i=0$) and the absence of the dissipation in the MQW ($\gamma_{\rm IT}=0$), the eigenmodes of this system are roots of the following secular equation:[7]

$$\frac{\omega^2}{c^2}=\frac{k_x^2}{\varepsilon_{zz}}+\frac{[k_z^{(i)}]^2}{\varepsilon_{xx}}=\frac{k_x^2+[k_z^{(i)}]^2}{\epsilon(\theta_i)}, \qquad (2)$$

where $k_z^{(i)}=(i+1)\pi/L_{\rm cav}$ $(i=0,1,2\ldots)$, $1/\epsilon(\theta_i)=\cos^2\theta_i/\varepsilon_{xx}+\sin^2\theta_i/\varepsilon_{zz}$, and $\theta_i=\arctan[k_x/k_z^{(i)}]$. Note that $\epsilon(\theta)$ can be treated as an angle variant effective dielectric function. At this point it is interesting to note that the concept of the angle variant dielectric function is often used in the literature.[10,11] Unfortunately, the expressions for $\epsilon(\theta)$, employed by the authors, are usually oversimplified.

Neglecting, for convenience, a small difference between the dielectric constant of the barrier material (ε_b) and the well material (ε_w), we find that[4] $\varepsilon_{zz}(\omega)=\varepsilon_w(\omega_{\rm IT}^2-\omega^2)/(\omega_{\rm IT}^2-\omega_p^2-\omega^2)$ (where $\omega_p^2=4\pi e^2\mathcal{N}_s/m^*\varepsilon_w L_{\rm MQW}$, m^* is the effective mass, and $L_{\rm MQW}$ is the period of the MQW). Substituting the above relations into Eq. (2), we get the following expression for the mode frequency as a function of k_x:

$$[\omega_{k_x,\pm}^{(i)}]^2=\frac{\omega_{\rm IT}^2+\omega_{k_x,c_i}^2}{2}\pm\sqrt{\frac{(\omega_{\rm IT}^2-\omega_{k_x,c_i}^2)^2}{4}+\mathcal{G}_{k_x,i}^2}, \qquad (3)$$

where $\omega_{k_x,c_i}=\omega_i^\perp/\cos\theta_i$, $\omega_i^\perp=k_z^{(i)}c/\sqrt{\varepsilon_w}$, and $\mathcal{G}_{k_x,i}=\omega_{k_x,c_i}\omega_p\sin\theta_i$.

It is instructive to discuss briefly the nonretarded limit ($c\to\infty$).[5] It is well known that in the case of bulk MQWs, the nonretarded Coulomb coupling leads to the delocalization of the intersubband plasmon modes and the formation of the intersubband plasmon band.[12] When the MQW thickness ($d_{\rm MQW}=L_{\rm cav}$) is finite, the mode frequencies (with fixed k_x) become discrete quantities. Making in Eq. (2) the substitution $c\to\infty$, one finds that the frequency of the Coulomb mode (denoted by $\mathcal{C}_\iota$, with $\iota=0,1,2\ldots$) is given by $\omega_{k_x,\mathcal{C}_\iota}=(\omega_{\rm IT}^2-\omega_p^2\sin^2\theta_\iota)^{1/2}$. The photonic and Coulomb modes with the same quantum number have the same oscillatory spatial dependence in the cavity. It is reasonable to treat the polariton branches $\omega_{k_x,+}^{(i)}$ and $\omega_{k_x,-}^{(i)}$ as a coherent mixture of the c_i and $\mathcal{C}_i$ modes.[6,9]

Since in the case of typical systems $\omega_p^2\ll\omega_{\rm IT}^2$, Eq. (3) can be approximated by

$$\omega_{k_x,\pm}^{(i)}=\frac{\omega_{\rm IT}+\omega_{k_x,c_i}}{2}\pm\frac{1}{2}\sqrt{(\omega_{k_x,c_i}-\omega_{\rm IT})^2+g_{k_x,i}^2}, \qquad (4)$$

where $g_{k_x,i}=\omega_p\sin\theta_i$. Deriving the above equation, we have assumed that ω_{k_x,c_i} is close to $\omega_{\rm IT}$, i.e., $k_x\approx k_{\rm res}^{(i)}\equiv[\omega_{\rm IT}^2-(\omega_i^\perp)^2]^{1/2}\sqrt{\varepsilon_w}/c$ or equivalently $\theta_i\approx\theta_{\rm res}^{(i)}\equiv\arccos(\omega_i^\perp/\omega_{\rm IT})$.

From Eq. (4) we find that the vacuum Rabi energy (defined as a half of the energy splitting in the absence of the dissipation[11]) can be written as $\hbar\Omega_{R_{\rm res}}^{(i)}=\frac{1}{2}\hbar\omega_p\sin\theta_{\rm res}^{(i)}$. It is instructive to show that the same result predicts a simple harmonic oscillator model (SHOM).[13] Following this model, we treat the intersubband electronic modes located in different QWs as independent oscillators having the same energy $E_{\rm IT}$. The electronic oscillator (located at $z=z_\kappa$, with $\kappa=1,2,3\ldots,N_{\rm QW}$) couples to the ith photonic oscillator (associated with c_i mode) with the position dependent strength $\bar{\mathcal{V}}_{k_x}^{(i)}(z_\kappa)=\mathcal{V}_{k_x}^{(i)}\Theta_\kappa^{(i)}$, where $\Theta_\kappa^{(i)}=\mathcal{E}_z^{(i)}(z_\kappa)/\mathcal{E}_z^{(i)}(z_{\rm max})$, $\mathcal{V}_{k_x}^{(i)}=\bar{\mathcal{V}}_{k_x}^{(i)}(z_{\rm max})$, $\mathcal{E}_z^{(i)}(z)$ is the normal component of the electric field associated with the c_i mode, and $z_{\rm max}^{(i)}$ is the antinode position of this field. The coupling constant $\mathcal{V}_{k_x}^{(i)}$ predicted by the quantum formalism can be expressed as $\mathcal{V}_{k_x}^{(i)}=(2L_{\rm MQW}/L_{\rm cav})^{1/2}V_{k_x}^{(i)}$ (provided that the antiresonant terms of light matter interaction are neglected).[9,11] Let us assume for simplicity that $k_x\approx k_{\rm res}^{(0)}$ and let us also take into account the c_0 photonic mode only. The SHOM leads then to the $(N_{\rm QW}-1)$-fold degenerate "dark" electronic eigenstates $\mathcal{D}_{\nu=1,2,3\ldots}$ with the energy $E_{\rm IT}$ and two split "bright" eigenstates.[13] The energies of the bright eigenstates are the same as the ones derived by diagonalizing a 2×2 Hamiltonian, in which two oscillators of energies $\hbar\omega_{k_x,c_0}$ and $E_{\rm IT}$ are coupled by an energy defined by $V_{k_x,i}^{\rm SHOM}=\{\sum_{\kappa=1}^{N_{\rm QW}}[\Theta_\kappa^{(i)}]^2\}^{1/2}\mathcal{V}_{k_x}^{(i)}$. Converting the summation to the integration and taking into account the standing wave character of the photonic modes,[9] we get the result $V_{k_x,i}^{\rm SHOM}\cong(N_{\rm QW}/2)^{1/2}\mathcal{V}_{k_x}^{(i)}=V_{k_x}^{(i)}$ equivalent to Eq. (4).

It is obvious that $(N_{\rm QW}-1)$ dark electronic states $\mathcal{D}_{\nu=1,2,3\ldots}$ can be chosen to be orthogonal to the bright state and to each other. (Here, in the considered simplified system the $\mathcal{D}_{\nu=1,2,3\ldots}$ states can be connected with the $\mathcal{C}_{\iota=1,2,3\ldots}$ states.) The dark electronic states come into play when higher cavity modes are included. Practically, the coupling between c_1 and $\mathcal{D}_1$ mode [leading to the formation of the mixed modes $\omega_{k_x,\pm}^{(1)}$] can be considered. It is connected with the fact that the coupling parameter $F_{\rm res}^{(i)}=g_{k_{\rm res}^{(0)},i}/2\delta_{\rm res}^{(i)}$ [with $\delta_{\rm res}^{(i)}=\omega_{k_{\rm res}^{(0)},c_i}-\omega_{\rm IT}$] decreases very fast by increasing the cavity mode number. Taking for estimation, the parameters consistent with the system studied in Fig. 1, namely: $\omega_0^\perp/\omega_{\rm IT}=0.3$ [$\delta_{\rm res}^{(1)}/\omega_{\rm IT}\approx0.13$] and $g_{k_{\rm res}^{(0)},0}/\omega_{\rm IT}=0.03$, we find that $F_{\rm res}^{(1)}$ is of the order 0.1. The low value of $F_{\rm res}^{(1)}$ implies that the branch $\omega_{k_x,-}^{(1)}$ [$\omega_{k_x,+}^{(1)}$] has nearly electronic (photonic) character and is located slightly below $\omega_{\rm IT}$ (above ω_{k_x,c_i}) at $k_x\approx k_{\rm res}^{(0)}$.

Note that usually the thickness of the MQW is substantially smaller than the effective thickness of the cavity. The role of the dark states in such systems can be analyzed qualitatively, replacing the MQW by the two QWs located at $z=z_1\equiv -L_{\mathrm{cav}}/2$ and $z=z_2\equiv z_1+d_{\mathrm{MQW}}$ and employing a 4×4 coupling Hamiltonian (see Ref. 14) in which the interaction between two lowest cavity modes and the above mentioned QWs is included. One finds that the role of the coupling between the c_1 mode and the dark mode decreases with a decrease in the ratio $d_{\mathrm{MQW}}/L_{\mathrm{cav}}$ and in the limit $d_{\mathrm{MQW}}\ll L_{\mathrm{cav}}$ can be completely neglected even when the ratio $\mathcal{V}_{k_x}^{(1)}/\delta_{\mathrm{res}}^{(1)}$ is comparable to unity.

Now, let us assume that the bottom mirror (separating the MQW and the substrate medium with $\varepsilon_s=\varepsilon_w$) has a very small but finite transmitivity $\mathcal{T}_b$. Then the coupling between the cavity mode and the external mode is possible, provided that both modes have the same frequency and the same in-plane wave vector k_x. In other words the external radiation propagating at the angle φ can only excite the confined modes, which are positioned in the $\omega-k_x$ plane at the intersection points of the line $\omega=k_x c/\sqrt{\varepsilon_w}\sin\varphi$ and the polariton branches $\omega_{k_x,\pm}^{(i)}$. [Note that not only the energies but also the wave vectors, $k_{x,\pm}^{(i)}$, corresponding to the above mentioned points are different.] One can check (taking for simplicity $\gamma_{\mathrm{IT}}=\mathcal{T}_b=0$) that the φ-dependent mode dispersion resulting from Eq. (2) takes the same form as Eq. (3) but with the following replacements: $\mathcal{G}_{k_x,i}\rightarrow\omega_p\omega_{\mathrm{IT}}\tan\varphi$ and $\omega_{k_x,c_i}^2\rightarrow\hat{\omega}_{c_i}^2=\omega_{c_i}^2+\omega_p^2\tan^2\varphi$, where $\omega_{c_i}=\omega_\perp^{(i)}/\cos\varphi$. Taking into account the dissipation and restricting to the case when $\omega_p^2\ll\omega_{\mathrm{IT}}^2$ and $\varphi\approx\varphi_{\mathrm{res}}^{(i)}$, we get the following dispersion equation for the constant angle radiative polaritons:

$$\tilde{\omega}_\pm^{(i)}(\varphi)=\frac{\tilde{\omega}_{\mathrm{IT}}+\tilde{\omega}_{c_i}}{2}\pm\frac{1}{2}\sqrt{(\tilde{\omega}_{c_i}-\tilde{\omega}_{\mathrm{IT}})^2+\omega_p^2\tan^2\varphi}. \quad (5)$$

Here $\tilde{\omega}_{\mathrm{IT}}=\omega_{\mathrm{IT}}-i\gamma_{\mathrm{IT}}$ and $\tilde{\omega}_{c_i}=\omega'_{c_i}-i\gamma_i$, where $\omega'_{c_1}=\omega_\perp^{(i)}/\cos\varphi$ and $\gamma_i=\gamma_i(\varphi)\approx\mathcal{T}_b\omega_\perp^{(i)}/4\pi\cos\varphi$. It is clear that the branch $\tilde{\omega}_-^{(0)}$ $[\tilde{\omega}_+^{(0)}]$, originating from the $\omega_{k_x,+}^{(0)}$ $[\omega_{k_x,-}^{(0)}]$ branch, can be associated with the L_0 (U_0) mode. The L_1 mode, can be connected with the $\tilde{\omega}_-^{(1)}$ branch [originating from the $\omega_{k_x,-}^{(1)}$ branch].

Inspection of Eq. (5) brings us to the important conclusion that the φ dependence of $\tilde{\omega}_+^{(i)}$ and $\tilde{\omega}_-^{(i)}$ can also be modeled by the two damped harmonic oscillators of energies $\tilde{\omega}_{\mathrm{IT}}$ and $\tilde{\omega}_{c_i}$ coupled by energy $V=\hbar\omega_p\tan\varphi$. It implies a simple relationship between the actual vacuum Rabi energy $\hbar\Omega_{R_{\mathrm{res}}}[\equiv V_{k_{\mathrm{res}}^{(0)},0}^{\mathrm{SHOM}}/2]$ and the minimum polariton splitting energy $[\Delta E_{\mathrm{min}}^{(0)}]$ observed in the ARRA spectra [at $\varphi=\varphi_{\mathrm{res}}^{(0)}$], namely, $\hbar\Omega_{R_{\mathrm{res}}}\approx\frac{1}{2}\Delta E_{\mathrm{min}}^{(0)}\cos\varphi_{\mathrm{res}}^{(0)}$. [We assume that $(\gamma_{\mathrm{IT}}-\gamma_0)^2\ll V^2\ll E_{\mathrm{IT}}^2$.] The above relation accurately reproduces the results presented in Fig. 1. It is also consistent with the results reported by Anappara *et al.* (see Fig. 4 of Ref. 11). At this point we would like to note that the φ-dependent dispersion derived by Pereira[10] overestimates (by a factor $\approx\sqrt{\varepsilon_w}/\sin\varphi$) the coupling energy and consequently the vacuum Rabi splitting energy.

Since the central mode is much more electronic than photonic, we can expect that its visibility should strongly depend on the transmitivity of the mirror.[9] The above statement is confirmed by numerical simulations based on the transfer-matrix method. They show that a relatively large value of the parameter γ_1 $(\gg\gamma_{\mathrm{IT}})$ and consequently a relatively low value of the Q_1 factor are required for the formation of the central peak in the ARRA spectra.

In conclusion, the numerical and analytical results presented in this Brief Report clearly demonstrate that the complex ARRA spectra of the BAMC with embedded MQW can be completely understood from the properties of the constant angle virtual modes supported by the system.

The work of M.Z. was partially supported by MNiSzW under the Grant No. N202 109 32/2854, 2007–2009.

[1] L. Wendler and T. Kraft, Phys. Rev. B **60**, 16603 (1999), and references therein.
[2] E. Dupont, H. C. Liu, A. J. SpringThorpe, W. Lai, and M. Extavour, Phys. Rev. B **68**, 245320 (2003).
[3] E. Dupont, J. A. Gupta, and H. C. Liu, Phys. Rev. B **75**, 205325 (2007).
[4] M. Załużny and C. Nalewajko, Phys. Rev. B **59**, 13043 (1999).
[5] R. Fuchs, K. L. Kliewer, and W. J. Pardee, Phys. Rev. **150**, 589 (1966).
[6] E. A. Vinogradov, Phys. Usp. **45**, 1213 (2002).
[7] M. Załużny, W. Zietkowski, and C. Nalewajko, Phys. Rev. B **65**, 235409 (2002).
[8] J. Plumridge, E. Clarke, R. Murry, and C. Phillips, Solid State Commun. **146**, 406 (2008).
[9] H. Zoubi and G. C. La Rocca, Phys. Rev. B **71**, 235316 (2005), and references therein.
[10] M. F. Pereira, Jr., Phys. Rev. B **75**, 195301 (2007).
[11] A. A. Anappara, A. Tredicucci, F. Beltram, G. Biasol, L. Sorba, S. De Liberato, and C. Ciuti, Appl. Phys. Lett. **91**, 231118 (2007), and references therein.
[12] A. C. Tselis and J. J. Quinn, Phys. Rev. B **29**, 3318 (1984).
[13] R. Houdre, R. P. Stanley, and M. Ilegems, Phys. Rev. A **53**, 2711 (1996).
[14] M. Richard, R. Romestain, R. Andre, and L. S. Dang, Appl. Phys. Lett. **86**, 071916 (2005).